processes

MDPI

Article

Thermal Characteristic Analysis of Sodium in Diluted Oxygen via Thermogravimetric Approach

Fang Chen, Xi-Lin Dong *, Yan Tang *, An-Chi Huang, Mei-Lin Zhang, Qing-Chun Kang, Zhong-Jun Shu and Zhi-Xiang Xing

School of Environmental and Safety Engineering, Changzhou University, Changzhou 213164, China; 19083700097@smail.cczu.edu.cn (F.C.); huangac@cczu.edu.cn (A.-C.H.); 19083700636@smail.cczu.edu.cn (M.-L.Z.); kangqingchun@cczu.edu.cn (Q.-C.K.); shuzhongjun@cczu.edu.cn (Z.-J.S.); xingzhixiang@cczu.edu.cn (Z.-X.X.)
* Correspondence: dongxl@cczu.edu.cn (X.-L.D.); tycd@cczu.edu.cn (Y.T.)

Abstract: As the main reactor type of the fourth-generation nuclear power systems, sodium-cooled fast reactors are now designed and built worldwide. A sodium pool cooling circulation process is indispensable in a sodium-cooled fast reactor. However, the sodium pool fire design is the basis of accidents in sodium-cooled fast reactors. The fire hazard caused by the sodium–oxygen reaction and fast reactor safety have attracted extensive attention. Dry powder is widely used as an effective fire-extinguishing agent to control sodium fire. The sodium will burn in an oxygen-depleted atmosphere when using dry powder to cover fire. In this study, the change law of thermogravimetry of melted sodium is studied by thermogravimetric analysis (TGA) and the apparent activation energy (E_a) is obtained, which has a linear relationship with the oxygen concentration. The results can provide a reference for improving the engineering design standards of sodium fire suppression systems and can also be incorporated into simulation software to improve the accuracy of fire suppression simulations.

Keywords: sodium oxygen reaction; sodium pool fire; thermogravimetric analysis; apparent activation energy; oxygen concentration

Citation: Chen, F.; Dong, X.-L.; Tang, Y.; Huang, A.-C.; Zhang, M.-L.; Kang, Q.-C.; Shu, Z.-J.; Xing, Z.-X. Thermal Characteristic Analysis of Sodium in Diluted Oxygen via Thermogravimetric Approach. *Processes* **2022**, *10*, 704. https://doi.org/10.3390/pr10040704

Academic Editor: Alfredo Iranzo

Received: 21 February 2022
Accepted: 4 April 2022
Published: 5 April 2022

1. Introduction

The concept of the fourth-generation nuclear reactor was proposed at the annual meeting of the American Nuclear Society in 1996. Not only are sodium-cooled fast reactors advanced, but they also possess advantages of safety and sustainability [1]. Therefore, they have excellent development potential. The small core volume and high thermal power rate of fast reactors necessitate a coolant with favourable heat transfer performance and weak neutron moderation [2]. Liquid sodium is therefore an ideal coolant for fast neutron reactors because it has a high thermal conductivity and functions over a wide temperature range (97.8–883 °C) [3], it can slow down the neutron velocity and hinder the chain reaction in the fast reactor; consequently, increasingly high pressure will not be generated in operation. At present, liquid sodium is an ideal coolant for fast neutron reactor.

The heat transfer system of the sodium-cooled fast reactor system consists of three parts [4]: the primary sodium circuit, the secondary sodium circuit, and the steam circulation system. The heat from the core is transferred to the secondary sodium circuit through the sodium in the primary sodium circuit, heating the make-up water in the steam circulation system, producing high-temperature and high-pressure steam, and promoting power generation. Subsequently, the cooled sodium flows back to the sodium pump and circulates again [5]; the details are shown in Figure 1. The sodium pool cooling circulation system is an irreplaceable part of the sodium-cooled fast reactor. However, the particular chemical property of sodium is its activity; it can easily react with oxygen. This characteristic determines its potential fire risk as a fast neutron reactor coolant, and its safety has attracted extensive attention.

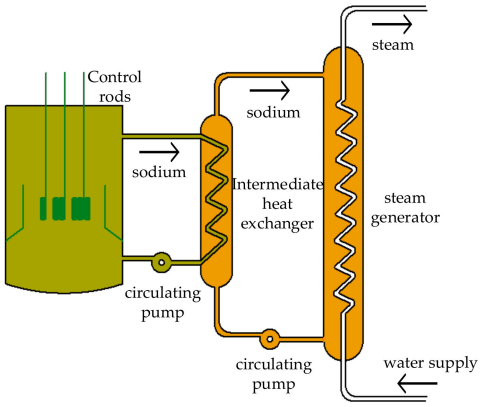

Figure 1. Schematic diagram of sodium-cooled fast reactor system.

Existing research has mainly focused on the combustion law of melted sodium in atmospheric air. Subramani [6] studied the diffusion of burning liquid sodium under isothermal and nonisothermal (burning) conditions. The results show that the nonisothermal effects of liquid sodium spreading can be neglected for the case of spreading or burning liquid sodium on a ground surface such as concrete or soil. Garcia [2] and Mitsuhiro Aoyagi [7] established the basic conservation equation of sodium pool flame combustion, and combined with the basic conservation formula of the simulation platform, established the numerical model of sodium pool flame combustion. Subsequent studies focused on the influence of sodium pool diameter and initial air temperature [8], the depth of sodium pool [9] on combustion speed, and the influence of oxygen concentration on fire time [10]. However, the influence of oxygen concentration on chemical reaction parameters and sodium activation energy (E_a) at the fire site has rarely been examined.

In a fire, the combustion mechanism of sodium fire will change greatly, regardless of whether inert gas (such as Ar or N_2) flooding fire extinguishing systems or dry powder fire extinguishing systems are used. These changes are especially pronounced when dry powder fire extinguishing agents are used [11]. Because of the barrier effect of the powder coating, airborne oxidants can only diffuse downward from the upper surface of the powder layer through the gaps between the powder particles. Meanwhile, the flame area on the liquid sodium surface is compressed by the dry powder layer and disappears. The sodium vapour on the surface of the liquid sodium diffuses upward slowly through the gaps between the powder particles and meets the oxidant in the powder, causing an oxidation reaction, and a flameless combustion zone is formed in the powder layer [12].

First, the variation in sodium thermogravimetry (TG), given by the first derivative of thermogravimetry (DTG) and combustion characteristic parameter (C_b) with temperature under different oxygen concentrations, is measured and calculated. Second, the E_a of sodium in each reaction stage is obtained by kinetic methods. Finally, the relationship between E_a and different oxygen concentrations is analyzed [13]. The research results of this study will help provide a deep understanding of sodium–oxygen reactions in sodium pool fire and provide a reference for sodium fire emergency fighting to stop accidents associated with sodium leakage fire and explosion.

2. Experimental and Methods

2.1. Materials

The sodium used in the present experiment was purchased from the Shanghai Titan Scientific Company, with a purity of 99.5% and of reagent grade quality. Sodium is a standard chemical reagent that can be prepared at a high-quality grade. The physical properties of sodium are listed in Table 1 [14]. Sodium is stored in a glove box filled with pure argon. Before the experiment, 1.7 ± 0.3 mg of sodium was placed in a supporting standard sapphire crucible (70 μL).

Table 1. Physical properties of sodium under standard pressure.

Physical Property	Numerical Value	Unit
Density	970 (20 °C); 784 (700 °C)	K/gm^3
Melting Point	98	°C
Boiling Point	881	°C
Molar Heat Capacity	28.23	J/(mol·°C)
Thermal Conductivity	142	W/(m·K)
Melting Heat	2.6	kJ/mol
Heat of Vaporization	101	kJ/mol

In instances of sodium leakage, sodium generates sodium oxide (Na_2O) by reacting with air. Under conditions of oxygen deficiency, the sodium–oxygen reaction mainly results in the formation of Na_2O.

$$2Na(l) + \frac{1}{2}O_2(g) \rightarrow Na_2O(S) \quad \Delta H = -416kJ/mol, \tag{1}$$

2.2. Thermogravimetric Analysis

TGA2 (produced by Mettler Toledo Co., Zurich, Switzerland) was used in the experiment. During the scan over the increase, the weight loss of sodium is obsevered, its thermal characteristics and changes are obtained by thermogravimetric analysis [15,16]. In this study, the experimental temperature range is from 30 to 600 °C, and the rates of heating (β) are 1, 3, 5, 7, and 9 °C/min, as planned. The test is conducted at a flow rate of 50 mL/min when the oxygen concentration is 4%, 8%, 16%, and 21%, as arranged, respectively [17].

3. Results and Simulation

3.1. Thermogravimetric Analysis

Thermogravimetric experiments obtained the TG and DTG curves in Figure 2 corresponding to the tested sodium samples with different oxygen concentrations at the rates of heating, as indicated.

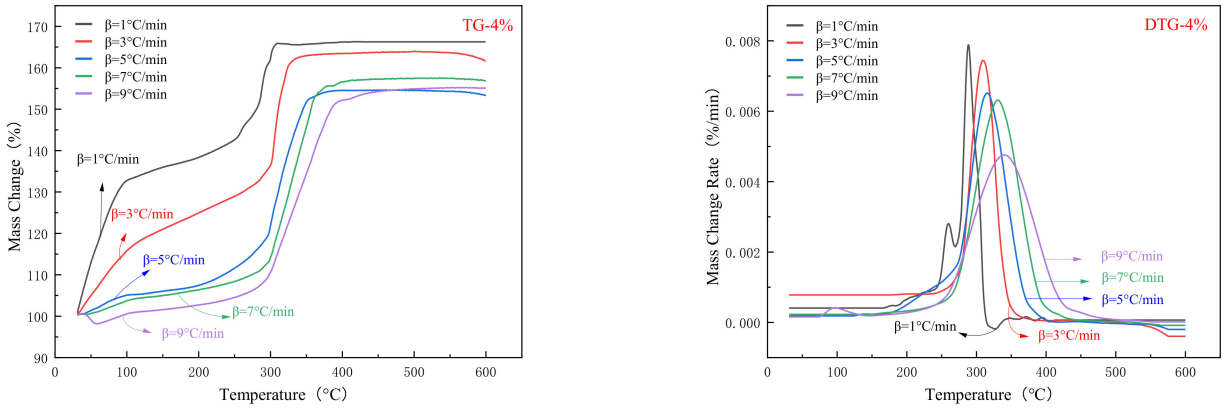

(**a**) (**b**)

Figure 2. *Cont.*

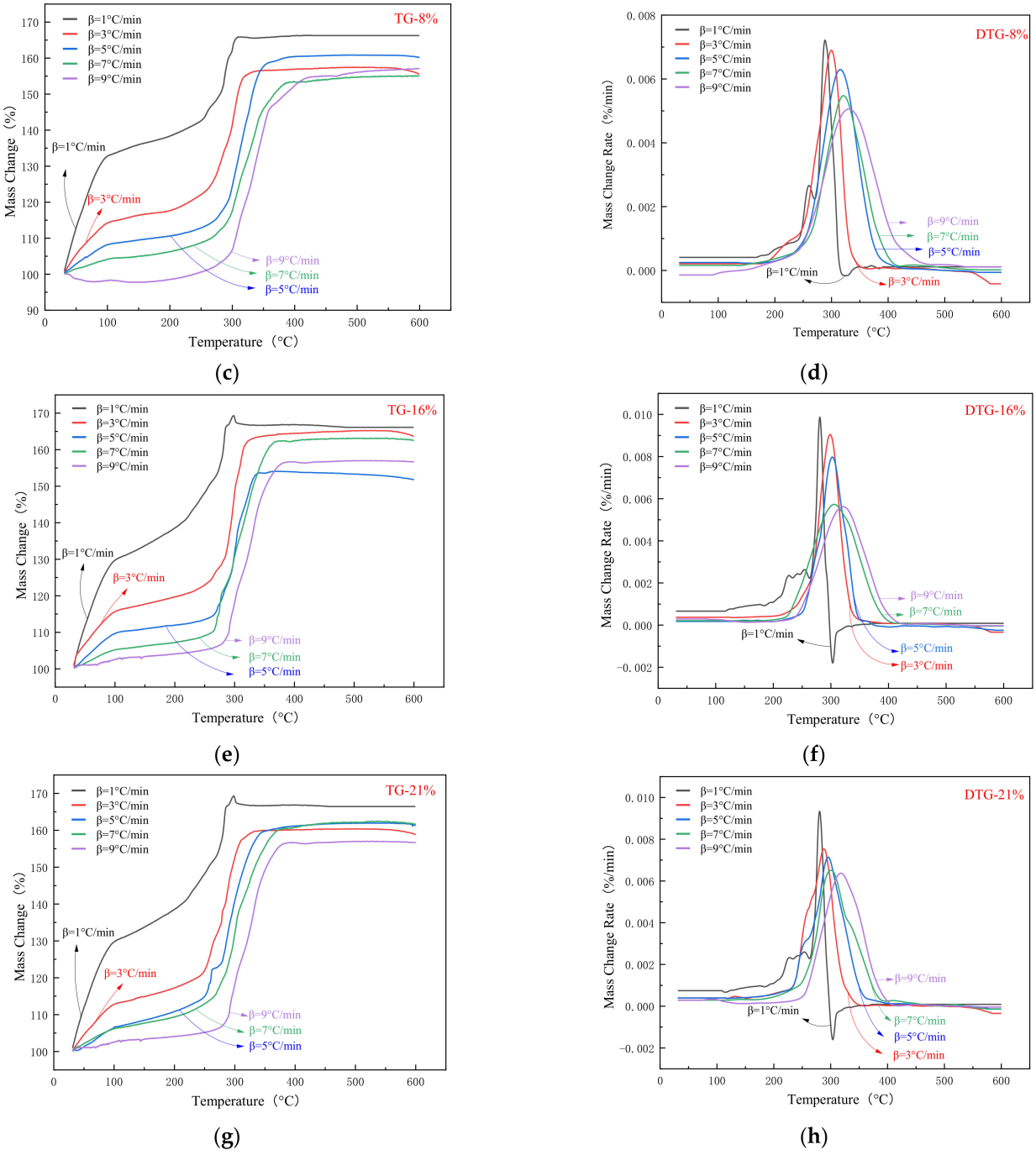

Figure 2. TG and DTG curves for sodium at oxygen concentrations of 4% (**a**,**b**), 8% (**c**,**d**), 16% (**e**,**f**), and 21% (**g**,**h**).

As indicated in Figure 2, TG and DTG in the oxidation process of sodium have the same overall change in trend, regardless of the experimental condition. The complete oxidation process can be divided into three stages:

1. Surface oxidation stage. TG curves are obtained in the temperature range of 30–100 °C. At this stage, the exothermic oxidation of sodium occurs and the mass increases substantially.
2. Stable endothermic stage. The mass increases slowly between 100 and 280 °C, and the heat release rate decreases in this stage because of the sodium oxide film that forms on the sodium surface in the initial stage, which hinders further oxidation.

3. Membrane rupture oxidation–combustion stage. The testing temperature is 280–350 °C, because the expansion coefficient of the sodium is greater than that of the external sodium oxide film; when sodium expands past a certain point, the generated expanding pressure leads to the rupture of the sodium oxide film formed at the earlier stage, and the uncovered sodium then continues to oxidize at higher temperatures, leading to rapid combustion and heat release from the exothermic reaction of the sodium [18–20].

In the DTG (b, d, f, and h) curves, due to the oxidation in the previous stage, the thick oxide film covering the sodium prevents further oxidation of the sodium, resulting in a slow increase in the surface layer thickness and an increase in the internal sodium heat absorption rate. The thermal curves show that the oxidation sequence of sodium repeats itself because of the exothermic oxidation of the surface. This sequence proceeds as follows: first, the coated sodium oxide undergoes endothermic weight gain; second, the sodium oxide film ruptures; and third, the bare sodium surface undergoes exothermic oxidation and endothermic melting [21,22]. Figure 3 summarizes the typical variation characteristics of TG and DTG in this testing process.

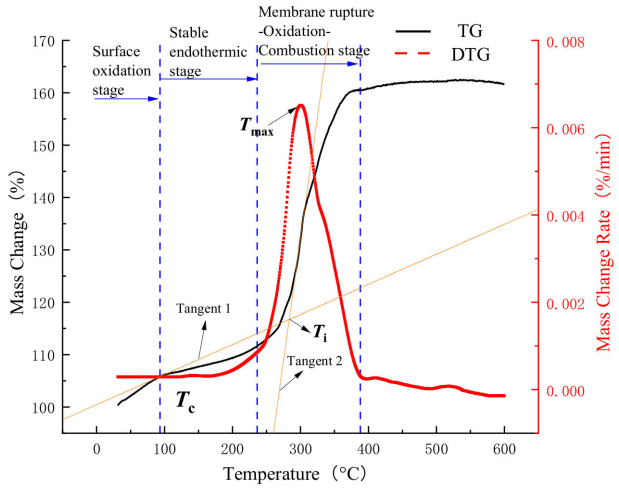

Figure 3. Typical characteristic curve of TG and DTG in the sodium oxidation reaction process.

T_c is the temperature corresponding to the highest point of oxygen absorption and weight gain stage. When the temperature reaches T_c, a dense oxide film has been formed on the surface of the sodium and limits the heat release rate of sodium later. T_{max} is the temperature corresponding to the peak value on the DTG curves, at which the reaction rate of the sodium reaches the maximum. T_i is the temperature of the oxide film rupture on the sodium surface; it is obtained by determining the intersection of two lines that are tangent to T_c and T_{max} on the TG curves (i.e., by using the extrapolation starting point method) [23]. For further quantitative analysis of the oxidation characteristics of sodium under different oxygen concentrations, the characteristic parameters in the reaction process were calculated, including the equilibrium temperature (T_h, °C) and maximum weight gain rate (d_{max}, %/min). Additionally, for better characterization of the oxidation combustion characteristics of sodium, a comprehensive index of combustion characteristic parameter C_b was also introduced into the analytical process, in which the surface oxide film rupture temperature and the maximum mass increase rate of sodium are integrated to characterize the combustion capacity of sodium pools formed in the later stages of the sodium reaction. The larger the value, the more favorable the performance [24],

$$C_b = 10^5 \frac{\left(\frac{d_w}{d_t}\right)_{max}}{T_{max}^2}, \quad (2)$$

where $(d_w/d_t)_{max}$ represents the maximum weight gain rate.

The characteristic parameter values of sodium reaction under different heating rates and different oxygen concentrations are obtained through calculation (Tables 2–5).

Table 2. Characteristic parameters of sodium–oxygen reaction at the oxygen concentration of 4%.

β (°C/min)	1	3	5	7	9
T_i (°C)	305.11	313.09	294.41	305.59	293.46
T_h (°C)	309.31	341.25	354.08	383.27	396.45
T_{max} (°C)	288.48	309.60	315.5	330.65	339.9
d_{max} (%/min)	0.22	0.52	0.59	0.78	0.86
C_b	0.26	0.54	0.59	0.71	0.74

Table 3. Characteristic parameters of sodium–oxygen reaction at the oxygen concentration of 8%.

β (°C/min)	1	3	5	7	9
T_i (°C)	311.08	299.6	305.43	293.14	298.56
T_h (°C)	310.45	336.70	361.50	388.98	420.90
T_{max} (°C)	288.60	299.80	315.58	320.97	330.6
d_{max} (%/min)	0.23	0.46	0.65	0.73	0.79
C_b	0.28	0.51	0.65	0.71	0.72

Table 4. Characteristic parameters of sodium–oxygen reaction at the oxygen concentration of 16%.

β (°C/min)	1	3	5	7	9
T_i (°C)	290.58	287.87	292.02	274.30	287.87
T_h (°C)	303.62	320.75	338.70	369.50	379.95
T_{max} (°C)	280.77	298.60	302.58	305.8	315.9
d_{max} (%/min)	0.24	0.51	0.63	0.78	0.88
C_b	0.30	0.57	0.69	0.83	0.88

Table 5. Characteristic parameters of sodium–oxygen reaction at the oxygen concentration of 21%.

β (°C/min)	1	3	5	7	9
T_i (°C)	266.32	271.91	281.33	286.43	311.17
T_h (°C)	303.03	332.65	347.33	373.47	385.65
T_{max} (°C)	280.45	287.85	295.583	300.2	317.40
d_{max} (%/min)	0.26	0.51	0.71	0.83	0.93
C_b	0.33	0.62	0.81	0.92	0.93

Comparing across Tables 2–5, the data show that at the same oxygen concentration, as β increases, the temperature of oxide film rupturing on the sodium surface, the equilibrium temperature at the later stage of oxidation combustion and combustion characteristic parameters increase when the sodium reaction rate reaches the maximum value. This indicates that temperature plays a substantial role in promoting sodium combustion. For example, in the Monju accident in Japan on 8 December, 1995, 640 kg of sodium vapour was sprayed out of the pipeline, sodium exposed to the air burned violently, sodium aerosol diffused rapidly, and the room temperature in the fire area soared to 1500 °C [25]. Therefore, once an accident occurs, the rapid increase in its heating rate will further accelerate sodium combustion.

As indicated by a longitudinal analysis of the data in the tables above, the temperature of each parameter decreases with oxygen concentration at the same heating rate. A simple calculation and conversion indicated that the time required to reach the characteristic parameter temperature is decreasing. When the oxygen concentration decreases from 21% to 16%, the change in the time required to meet each parameter is relatively small, but this time changes greatly when the oxygen concentration decreased from 16% to 8%. For example, for the maximum increasing temperature (T_{max}), when the heating rate is 5 °C/min, the time difference required for the oxygen concentration to decrease from 21% to 16% is 84 s; while the time needed for the oxygen concentration to reduce from 16% to 8% is 156 s, an interval 186% greater than the decrease from 21% to 16%. The critical point of maximum combustion increase is the temperature at which the ultimate weight gain rate reaches the maximum value under the competing action of sodium melting and oxidation. The time required to achieve this temperature increases slowly from an oxygen concentration of 21% to an oxygen concentration of 16%, but then rapidly increases from a concentration of 16% to an oxygen concentration of 8%, indicating that the oxidation combustion intensity of sodium is greatly weakened.

3.2. Nonisothermal Kinetic Analysis

3.2.1. Thermal Analysis Method

In 1920, the emergence of thermal analysis methods led to the gradual emergence of the study of material reaction kinetics and was further developed in the 1950s. The study of kinetic methods in thermal analysis reflects the researchers' pursuit of the essence of complex concepts and the continued perfection of kinetic research theory. This research encompasses from the kinetic equations of homogeneous isothermal reaction to the heterogeneous nonisothermal reaction systems, and from simple kinetic approaches to complex designs. Thermal analysis kinetics is a process in which various calorimetric instruments are used to determine the changes that can be detected at different thermal parameters in the reaction system, following which kinetic reaction parameters are determined through a series of analyses according to the changes in the aforementioned parameters. In this study, the Kissinger method is used to process the experimental data [26–29].

3.2.2. Kissinger Method

The Kissinger method [30], also known as a maximum method, is used to calculate the value of E_a, which can be expressed as:

$$\ln\left(\frac{\beta}{T_m^2}\right) = \ln\left[-\frac{AR}{E_a}f'(\alpha_m)\right] - \frac{E_a}{RT_m}, \quad (3)$$

According to formula (3), take $\ln\left(\frac{\beta}{T_P^2}\right)$, plot $1/T_P$, and calculate E_a according to the slope and intercept of the straight line [31,32].

3.3. Relationship between E_a and Oxygen Concentration

As shown in Figure 4, the E_a decreases with the decrease in oxygen concentration, mainly because the progress of the sodium–oxygen reaction is related to oxygen partial pressure.

The above conclusions can be explained by the oxygen diffusion-based model [8]. In this approach, it is assumed that the sodium–air reaction is infinitely fast and occurs at the pool surface. This means that the oxygen concentration at the pool surface is zero. A two-step oxidation mechanism is assumed for the sodium–air reaction with sodium oxide and sodium dioxide as the byproducts, which is given as follows:

$$aNa(g) + bO_2(g) \rightarrow (1-s)Na_2O(s) + sNa_2O_2(s) + H_c, \quad (4)$$

where a and b are stoichiometric coefficients of sodium and oxidizer, s is the stoichiometric ratio, and H_c is heat of combustion in J/kg.

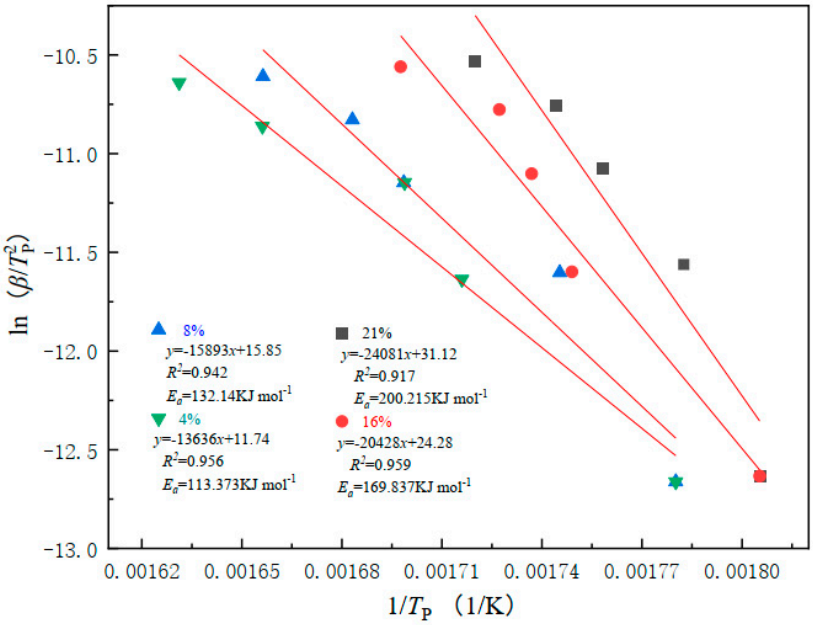

Figure 4. Solution of E_a of sodium at different oxygen concentrations using Kissinger method.

The oxygen diffusion-based model described above is validated against the sodium pool experiments of Newman and Payne [33]. They conducted sodium pool combustion experiments in an ambient environment with three different initial oxygen concentrations, 4%, 9.5%, and 21% (by vol.). The results obtained using the oxygen diffusion-based model are in good agreement with the experiments. At lower oxygen concentrations, only sodium monoxide is present, which means that the stoichiometric ratio is 0, while at higher oxygen concentrations, Na_2O further reacts to form Na_2O_2, which means that the stoichiometric ratio is 1. As a consequence, with the increase in oxygen concentration, the sodium–oxygen reaction will more easily generate sodium peroxide, since sodium peroxide is more stable than sodium oxide, it will hinder the progress of the sodium–oxygen reaction, and the value of E_a increases accordingly.

E_a and oxygen concentration calculated using the Kissinger method (Figure 5) were linearly related by the best-fit equation:

$$Ea = 5.06x + 91.87, \quad (5)$$

where x (in %) is the oxygen concentration.

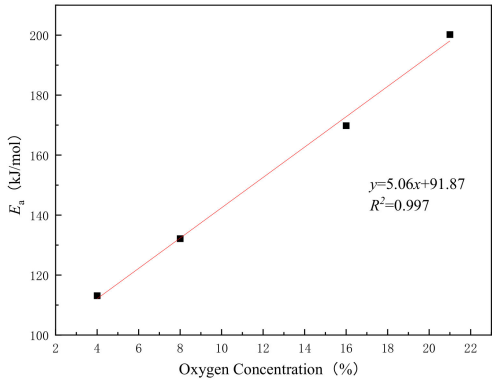

Figure 5. Linear relationship between E_a of sodium and oxygen concentration.

4. Conclusions

This study analyzed the complete process of the oxidative combustion of sodium at different oxygen concentrations using TG. The changes in TG, DTG, and reaction characteristic parameters are analyzed with heating rate and oxygen concentration. The E_a of oxidative sodium combustion is calculated by using the Kissinger method, and the relationship of E_a with oxygen concentration is determined. The main conclusions are as follows:

1. As indicated by the TG curve, the complete oxidation combustion process of sodium can be divided into three stages. These stages are the surface oxidation stage, which occurs in the temperature range from 30 to 100 °C; the stable endothermic stage, which occurs in the temperature range from 100 to 280 °C; and the membrane rupture oxidation combustion stage, which occurs at the temperature range from 280 to 350 °C.
2. At the same oxygen concentration, as the heating rate increases, increases were also noted in the temperature of the oxide film rupture on the sodium surface, in the temperature when the sodium reaction rate reaches the maximum, in the equilibrium temperature in the later stages of oxidation combustion, and in the combustion characteristic parameters; all showed an upward trend. Conversely, at the same heating rate, with the decrease in oxygen concentration, the time required to reach the characteristic parameter temperature increases and changes greatly when the oxygen concentration decreases from 16% to 8%;
3. The E_a of different oxygen concentrations is calculated by the Kissinger method, and the E_a decreases with decreases in oxygen concentration, mainly because the progress of the sodium–oxygen reaction is related to the partial pressure of oxygen. E_a was linearly related to oxygen concentration. Under certain other conditions, at higher oxygen concentrations, the reaction of Na_2O formation was more inhibited and the sodium pool fire more easily formed highly toxic combustion products of aerosols.

Therefore, at the early stages of sodium leakage, immediate measures should be implemented to prevent the generation of corrosive aerosols from damaging the sodium-cooled fast reactor and causing more serious accidents. In addition, it provides a theoretical basis for the preparation of fire extinguishing system engineering design and sodium fire emergency rescue guide, and meets the needs of sodium-cooled fast reactor engineering construction.

Author Contributions: Conceptualization, F.C.; methodology, Y.T. and A.-C.H.; validation, Z.-J.S. and M.-L.Z.; formal analysis, M.-L.Z. and F.C.; resources, Q.-C.K.; writing—original draft preparation, F.C.; writing—review and editing, Y.T. and A.-C.H.; project administration, X.-L.D. and Z.-X.X.; funding acquisition, X.-L.D. and Z.-X.X. All authors have read and agreed to the published version of the manuscript.

Funding: This work was supported by the Science and Technology Plan Project of Fire Rescue Bureau of Emergency Management Department (grant number 2021XFCX18); Jiangsu Province Postgraduate Research and Practice Innovation Project (grant number KYCX21_2879); and General Natural Science Research Project of Jiangsu Universities in 2020 (No. 20KJB620002).

Institutional Review Board Statement: Not applicable.

Informed Consent Statement: Not applicable.

Conflicts of Interest: The authors declare no conflict of interest.

References

1. Ge, L.; Lu, T.; Shan, J.; Liu, D. Application of a 3D model in the transient system analysis of sodium-cooled fast reactor. *Ann. Nucl. Energy* **2020**, *135*, 106967. [CrossRef]
2. Garcia, M.; Herranz, L.E.; Kissane, M.P. Theoretical assessment of particle generation from sodium pool fires. *Nucl. Eng. Des.* **2016**, *310*, 470–483. [CrossRef]
3. Lebel, L.S.; Girault, N. Aerosol generation from sodium pool fires: Learning from the 1980s-era EMIS experiments and modelling. *Nucl. Eng. Des.* **2018**, *330*, 36–50. [CrossRef]

4. Sungjoo, L.; Byungun, Y.; Juneseuk, S. Effects of Nuclear Energy on Sustainable Development and Energy Security: Sodium-Cooled Fast Reactor Case. *Sustainability* **2016**, *8*, 979.
5. Kim, M.H.; Nguyen, V.T.; Im, S.; Jung, Y.; Kim, B.J. Experimental Validation of Flow Uniformity Improvement by a Perforated Plate in the Heat Exchanger of SFR Steam Generator. *Energies* **2021**, *14*, 5846. [CrossRef]
6. Subramani, A.; Jayanti, S.; Shet, U.S.P.; Selvaraj, P. Dynamics of liquid sodium pool spreading under sodium fire conditions. *Nucl. Eng. Des.* **2009**, *239*, 1354–1361. [CrossRef]
7. Aoyagi, M.; Uchibori, A.; Kikuchi, S.; Takata, T.; Ohno, S.; Ohshima, H. Identification of important phenomena through the PIRT process for development of sodium fire analysis codes. *Nucl. Eng. Des.* **2019**, *353*, 110240. [CrossRef]
8. Sathiah, P.; Roelofs, F. Numerical modeling of sodium fire—Part II: Pool combustion and combined spray and pool combustion. *Nucl. Eng. Des.* **2014**, *278*, 739–752. [CrossRef]
9. Subramani, A.; Jayanti, S. Experimental studies on burning behaviour of liquid sodium in a shallow pool. *Nucl. Eng. Des.* **2010**, *240*, 3462–3466. [CrossRef]
10. Makino, A.; Fukada, H. Ignition and combustion of a falling, single sodium droplet. *Proc. Combust. Inst.* **2005**, *30*, 2047–2054. [CrossRef]
11. An, D.; Sunderland, P.B.; Lathrop, D.P. Suppression of sodium fires with liquid nitrogen. *Fire Saf. J.* **2013**, *58*, 204–207. [CrossRef]
12. Nur, K.; Laurent, B.; Thierry, G.; Cendrine, G.; Henri, B. The role of powder physicochemical properties on the extinction performance of an extinguishing powder for sodium fires. *Nucl. Eng. Des.* **2019**, *346*, 24–34. [CrossRef]
13. Xn, A.; Zhong, Z.B. Extinguishment of sodium fires with Graphite@Stearate core-shell structured particles. *Fire Saf. J.* **2019**, *111*, 102933.
14. Saravanan, S.M.; Rao, P.M.; Raghupathy, S. Analysis of liquid sodium spills spreading on floor surface pertaining to sodium pool fire events in SFR cells. *Nucl. Eng. Des.* **2020**, *363*, 110614. [CrossRef]
15. Wang, J.; Jia, H.; Tang, Y.; Xiong, X.; Ding, L. Thermal stability and non-isothermal crystallization kinetics of metallocene poly (ethylene-butene-hexene) /high fluid polypropylene copolymer blends. *Thermochim. Acta* **2017**, *647*, 55–61. [CrossRef]
16. Tsai, Y.T.; Liao, J.Y.; Shu, C.M. Explosion characteristics of chlorodifluoromethane and isobutane at high temperature and pressure using a 20-L apparatus. *Int. J. Refrig.* **2018**, *96*, 155–160. [CrossRef]
17. Yang, M.; Chen, X.; Wang, Y.; Yuan, B.; Niu, Y.; Zhang, Y.; Liao, R.; Zhang, Z. Comparative evaluation of thermal decomposition behavior and thermal stability of powdered ammonium nitrate under different atmosphere conditions. *J. Hazard. Mater.* **2017**, *337*, 10–19. [CrossRef]
18. Jeurgens, L.; Sloof, W.; Tichelaar, F.; Mittemeijer, E. Thermodynamic stability of amorphous oxide films on metals: Application to aluminum oxide films on aluminum substrates. *Phys. Rev. B* **2000**, *62*, 4707–4719. [CrossRef]
19. Wang, Q.; Shen, Z.; Jiang, J.; Wang, Q.; Shu, C.M.; Sun, Y.; Wang, L. Suppression effects of ammonium dihydrogen phosphate dry powder and melamine pyrophosphate powder on an aluminium dust cloud explosion. *J. Loss Prev. Process Ind.* **2020**, *68*, 104312. [CrossRef]
20. Hasani, S.; Soleymani, A.P.; Panjepour, M.; Ghaei, A. A Tension Analysis During Oxidation of Pure Aluminum Powder Particles: Non-isothermal Condition. *Oxid. Met.* **2014**, *82*, 209–224. [CrossRef]
21. Rosenband, V. Thermo-mechanical aspects of the heterogeneous ignition of metals. *Combust. Flame* **2004**, *137*, 366–375. [CrossRef]
22. Trunov, M.A.; Schoenitz, M.; Dreizin, E. Ignition of Aluminum Powders Under Different Experimental Conditions. *Propellants Explos. Pyrotech.* **2005**, *30*, 36–43. [CrossRef]
23. Mahidin; Usui, H.; Ishikawa, S.; Hamdani. The Evaluation of Spontaneous Combustion Characteristics and Properties of Raw and Upgraded Indonesian Low Rank Coals. *Coal Prep.* **2002**, *22*, 81–91. [CrossRef]
24. Xu, C.; Sun, X. Combustion characteristic of biomass by using TG-DTG-DSC thermoanalysis. *J. Huazhong Univ. Sci. Technol. Nat. Sci. Ed.* **2007**, *3*, 126–128.
25. Makino, A. Ignition Delay and Limit of Ignitability for Sodium Pool (Theory and Experimental Comparisons). *JSME Int. J. Ser. B Fluids Therm. Eng.* **2006**, *49*, 92–101. [CrossRef]
26. National Fire Protection Association. *Fire Protection Guide on Hazardous Materials*; National Fire Protection Association: Quincy, MA, USA, 1972.
27. Anderson, O.L.; Stuart, D.A. Calculation of Activation Energy of Ionic Conductivity in Silica Glasses by Classical Methods. *J. Am. Ceram. Soc.* **2010**, *37*, 573–580. [CrossRef]
28. Xie, L.-J.; Jiang, J.-C.; Huang, A.-C.; Tang, Y.; Liu, Y.-C.; Zhou, H.-L.; Xing, Z.-X. Calorimetric Evaluation of Thermal Stability of Organic Liquid Hydrogen Storage Materials and Metal Oxide Additives. *Energies* **2022**, *15*, 2236. [CrossRef]
29. Huang, A.-C.; Chuang, Y.-K.; Huang, C.-F.; Shu, C.-M. Thermokinetic analysis of the stability of malic and salicylic acids in cosmeceutical formulations containing metal oxides. *J. Therm. Anal. Calorim.* **2018**, *132*, 165–172. [CrossRef]
30. Xu, X.; Pan, R.; Chen, R. Comparative Thermal Degradation Behaviors and Kinetic Mechanisms of Typical Hardwood and Softwood in Oxygenous Atmosphere. *Processes* **2021**, *9*, 1598. [CrossRef]
31. Farjas, J.; Roura, P. Exact analytical solution for the Kissinger equation: Determination of the peak temperature and general properties of thermally activated transformations. *Thermochim. Acta* **2014**, *598*, 51–58. [CrossRef]
32. Vyazovkin, S. Kissinger Method in Kinetics of Materials: Things to Beware and Be Aware of. *Molecules* **2020**, *25*, 2813. [CrossRef] [PubMed]
33. Newman, R.N.; Payne, J. The burning rates of sodium pool fires. *Combust. Flame* **1978**, *33*, 291–297. [CrossRef]